

---

This is an electronic reprint of the original article.

This reprint may differ from the original in pagination and typographic detail.

Kuznetsov, Nikolai; Qin, Huajun; Flajsman, Lukas; van Dijken, Sebastiaan

**Tuning of spin-wave transmission and mode conversion in microscopic YIG waveguides with magnonic crystals**

*Published in:*  
Journal of Applied Physics

*DOI:*  
[10.1063/5.0123234](https://doi.org/10.1063/5.0123234)

Published: 15/11/2022

*Document Version*  
Publisher's PDF, also known as Version of record

*Please cite the original version:*

Kuznetsov, N., Qin, H., Flajsman, L., & van Dijken, S. (2022). Tuning of spin-wave transmission and mode conversion in microscopic YIG waveguides with magnonic crystals. *Journal of Applied Physics*, 132(19), Article 193904. <https://doi.org/10.1063/5.0123234>

# Tuning of spin-wave transmission and mode conversion in microscopic YIG waveguides with magnonic crystals


Cite as: J. Appl. Phys. **132**, 193904 (2022); <https://doi.org/10.1063/5.0123234>

Submitted: 29 August 2022 • Accepted: 27 October 2022 • Published Online: 15 November 2022

Nikolai Kuznetsov, Huajun Qin,  Lukáš Flajšman, et al.

## COLLECTIONS

Paper published as part of the special topic on [Recent Advances in Magnonics](#)

 This paper was selected as Featured



View Online



Export Citation



CrossMark

## ARTICLES YOU MAY BE INTERESTED IN

### Hybrid magnonic-oscillator system

Journal of Applied Physics **132**, 183904 (2022); <https://doi.org/10.1063/5.0123471>

### Introduction to spin wave computing

Journal of Applied Physics **128**, 161101 (2020); <https://doi.org/10.1063/5.0019328>

### Dipole-exchange spin waves in unsaturated ferromagnetic nanorings with interfacial Dzyaloshinski-Moriya interactions

Journal of Applied Physics **132**, 193901 (2022); <https://doi.org/10.1063/5.0121913>



## APL Quantum

**CALL FOR APPLICANTS**

## Seeking Editor-in-Chief

# Tuning of spin-wave transmission and mode conversion in microscopic YIG waveguides with magnonic crystals

Cite as: J. Appl. Phys. **132**, 193904 (2022); doi: [10.1063/5.0123234](https://doi.org/10.1063/5.0123234)

Submitted: 29 August 2022 · Accepted: 27 October 2022 ·

Published Online: 15 November 2022



Nikolai Kuznetsov,<sup>1</sup> Huajun Qin,<sup>2,3,a)</sup> Lukáš Flajšman,<sup>1</sup>  and Sebastiaan van Dijken<sup>1,a)</sup> 

## AFFILIATIONS

<sup>1</sup>NanoSpin, Department of Applied Physics, Aalto University School of Science, FI-00076 Aalto, Finland

<sup>2</sup>School of Physics and Technology, Wuhan University, Wuhan 430072, China

<sup>3</sup>Wuhan Institute of Quantum Technology, Wuhan 430206, China

**Note:** This paper is part of the Special Topic on Recent Advances in Magnonics.

**a) Authors to whom correspondence should be addressed:** [qinhua@whu.edu.cn](mailto:qinhua@whu.edu.cn) and [sebastiaan.van.dijken@aalto.fi](mailto:sebastiaan.van.dijken@aalto.fi)

## ABSTRACT

We report experimental results on spin-wave propagation, transmission gap tuning, and mode conversion in straight, curved, and Y-shaped yttrium iron garnet waveguides with magnonic crystals made of submicrometer-wide airgrooves. We observe forbidden frequency gaps with sizes up to 200 MHz in straight waveguides and narrowing of the gaps in curved and Y-shaped waveguides. The spin-wave transmission signal is strongly suppressed inside the gaps and remains high at allowed frequencies for all waveguide types. Using super-Nyquist sampling magneto-optical Kerr effect microscopy, we image symmetric and asymmetric spin-wave interference patterns, the self-focusing of propagating spin waves, and interconversions between width modes with different quantization numbers.

Published under an exclusive license by AIP Publishing. <https://doi.org/10.1063/5.0123234>

## I. INTRODUCTION

Active manipulation of spin-wave transport is essential for magnonic technologies that utilize spin waves for energy-efficient data transfer, storage, and information processing.<sup>1–7</sup> Magnonic crystals, artificially designed magnetic metamaterials, are commonly used to control spin-wave transmission signals. The band structure of a magnonic crystal consists of allowed minibands and forbidden frequency gaps where the propagation of spin waves is strongly suppressed. Yttrium iron garnet (YIG) is a good material for magnonic crystals because of its ultralow magnetic damping. Previous studies have focused on micrometer-thick YIG magnonic crystals made of periodic airgrooves,<sup>8–10</sup> width modulations,<sup>11–13</sup> and patterned metallic stripes on top.<sup>14–16</sup> Active manipulation of spin-wave transport properties by an electric current,<sup>17,18</sup> strain,<sup>19</sup> or voltage<sup>20–24</sup> has also been demonstrated. In previous, we have shown that nanometer-thick YIG films with only two to six airgrooves do also possess properties of a magnonic crystal if the airgrooves have considerable depth in comparison with the film thickness.<sup>25,26</sup> Because of efficient spin-wave scattering in this type

of periodic structure, the transmission gaps are tuned effectively by varying the groove depth, lattice constant, and film thickness. However, nanometer-thick YIG magnonic crystals have been fabricated by patterning microscopic waveguides with regular width modulations.<sup>13</sup> Different from continuous films, the interference of multiple width modes in magnonic waveguides leads to the self-focusing of propagating spin waves.<sup>27</sup> Because YIG waveguides are essential for magnonic devices,<sup>28–33</sup> it is of interest to characterize spin-wave transport in microscopic waveguides with deep airgrooves.

Here, we report on the spin-wave properties of nanometer-thick YIG magnonic waveguides with submicrometer-wide deep airgrooves. We study three different waveguide structures: straight, curved, and Y-shaped. The broadband spin-wave spectra of all waveguides exhibit deep transmission gaps. The gap width is ~200 MHz for the straight waveguide and ~100 MHz for the curved and Y-shaped structures. Using super-Nyquist-sampling magneto-optical Kerr effect (SNS-MOKE) microscopy, we map the transmission of symmetric and asymmetric width modes and

interconversions between modes with odd and even quantization numbers.

## II. EXPERIMENTAL DETAILS

In the experiments, 50-nm-thick YIG films were grown on (111)-oriented, single-crystal  $\text{Gd}_3\text{Ga}_5\text{O}_{12}$  (GGG) substrates by pulsed laser deposition. Before growth, the GGG substrates were cleaned in acetone and isopropanol using an ultrasonic bath and degassed at 500°C for 10 min in the vacuum deposition chamber. After this, the substrate was heated to 850°C with a ramp rate of 5°C/min in  $\text{O}_2$  atmosphere with pressure  $p_{\text{O}_2} = 0.13$  mbar. The YIG film was deposited using an excimer laser with a pulse repetition rate of 2 Hz and a fluence of 1.8 J/cm<sup>2</sup>. After film growth, the samples were annealed *in situ* at 750°C for 10 min at  $p_{\text{O}_2} = 13$  mbar followed by cooling to room temperature with a rate of −3°C per minute. We measured the ferromagnetic resonance (FMR) of as-grown YIG films. By fitting the FMR linewidth as a function of frequency, we extracted a Gilbert damping constant of  $(6.2 \pm 1.2) \times 10^{-4}$ . We used laser-writing and argon-ion milling techniques to pattern the YIG film into 10-μm-wide waveguides. Periodic airgrooves forming the magnonic crystals were patterned into the waveguide by electron beam lithography (EBL) and argon-ion milling. The airgroove depth was 15 nm. To excite spin waves, 1 μm-wide antennas made of 3 nm Ta/140 nm Au were patterned using EBL and lift-off. The distance between the two parallel antennas was 100 μm. We characterized spin-wave transport using broadband spin-wave spectroscopy and SNS-MOKE microscopy. The spectroscopy setup consisted of a two-port vector network analyzer and a home-built electromagnet probing station. Spin-wave transmission spectra were measured by recording the  $S_{12}$  scattering parameter. We used a frequency sweep method to record spectra for different magnetic bias fields. To improve contrast, a reference spectrum taken at 150 mT was subtracted from the measurement data. In the SNS-MOKE technique, the laser frequency comb downconverts the excited spin waves to an intermediate frequency  $\varepsilon$ , allowing tuning of the excitation signal to any frequency  $f_{\text{exc}} = n \times f_{\text{rep}} + \varepsilon$ . With the excitation synchronized to a laser repetition rate of  $f_{\text{rep}} = 80$  MHz and non-zero  $\varepsilon$ , the spin-wave phase relative to the excitation signal is preserved by lock-in demodulation at  $\varepsilon$ .<sup>34</sup> The demodulated signal carries information about the amplitude and phase of the propagating spin waves. The excitation power of the microwave signal was set at −10 dBm in both the broadband spin-wave spectroscopy and SNS-MOKE microscopy experiments to ensure that all measurements are conducted in the linear regime.

## III. RESULTS AND DISCUSSIONS

Figures 1(a)–1(c) show schematics of the measurement geometry including the microwave antennas and the straight, curved, and Y-shaped waveguides with magnonic crystals made of three airgrooves. The lattice constant of the crystals is  $a = 2$  μm, the groove depth is  $d = 15$  nm, and the groove width is  $w = 500$  nm. The angle of the curves in the curved and Y-shaped structures with respect to the  $x$  axis is 15°, which is well below the calculated 68° cut-off angle for surface spin waves.<sup>35</sup> The magnonic crystals are positioned in the center of the curved arms. During the

measurements, an external magnetic bias field saturates the magnetization of the YIG waveguides along the  $y$  axis. Consequently, the spin waves propagate in the Damon–Eshbach (DE) configuration in the straight parts of the structures, while the magnetization is tilted 15° away from this geometry in the waveguide curves. Figures 1(d)–1(f) depict contour plots of the  $S_{12}$  scattering parameter amplitude as a function of magnetic bias field. The measured broadband spin-wave transmission spectra exhibit two deep frequency gaps for all waveguides. Within the gaps, strong spin-wave rejection lowers the transmission signal to the measurement background level. In contrast, spin waves at allowed frequencies efficiently transmit between the two antennas [the  $S_{12}$  amplitude is comparable to the reference signal measured on a bare YIG waveguide without magnonic crystal, see blue line in Fig. 1(g)]. Weakening of the spin-wave excitation efficiency gradually reduces the transmission signal with increasing frequency.

Figures 1(g)–1(i) display  $S_{12}$  line profiles for an external bias field of 15 mT (orange lines). The transmission gaps are measured at frequencies corresponding to  $k = m\pi/a$ , where  $m$  is the order number of the rejection band. To illustrate this, we calculated the dispersions of the fundamental spin-wave mode for the straight, curved, and Y-shaped parts of the waveguides using the Kalinikos–Slavin model,<sup>36,37</sup>

$$f = \frac{\gamma\mu_0}{2\pi} \sqrt{\frac{(H_{\text{eff}} + M_{\text{eff}}(1 - p + \lambda_{\text{ex}}^2 k^2))}{(H_{\text{eff}} + M_{\text{eff}}(p \frac{k_x^2}{k^2} + \lambda_{\text{ex}}^2 k^2))}}. \quad (1)$$

Here,  $p = 1 - (1 - e^{-kt})/kt$ ,  $k^2 = k_x^2 + k_y^2$ , and  $\lambda_{\text{ex}} = (2A/M_{\text{eff}}^2)^{1/2}$  is the exchange length. In the calculations, we used the long-wave approximation ( $kt \ll 1$ ) and assumed unpinned surface spins. The effective magnetic field in the straight and curved parts of the waveguides was simulated in MuMax3.<sup>38</sup> Moreover, we used parameters  $\frac{\gamma}{2\pi} = 28$  GHz/T,  $t = 50$  nm, and  $M_{\text{eff}} = 170$  kA/m (extracted from FMR measurements). Dispersion curves for the straight, curved, and Y-shaped parts of the YIG waveguides are shown as orange lines in the right panels of Figs. 1(g)–1(i). The effective magnetic field in the two curves of the Y-shaped waveguide is similar, leading to nearly identical spin-wave dispersions in the two legs of this structure as well as in the waveguide with a single curve. Besides calculations, we also extracted spin-wave dispersion data from SNS-MOKE microscopy experiments on the straight waveguide [Fig. 1(g)]. The measured gap frequencies in the spin-wave transmission spectra agree with the predicted ones based on the calculated and measured dispersions and  $k = m\pi/a$  with  $a = 2$  μm.

Next, we compare the center frequency and gap size of the first transmission gap for the straight, curved, and Y-shaped waveguides, as shown in Fig. 2. The gap size is extracted at the maximum intensity of the second allowed miniband [see arrows in Figs. 1(g)–1(i)]. The bandgap center frequency is nearly the same for all waveguides and follows the YIG dispersion curves with increasing bias field. However, the gap size of the straight waveguide is about two times larger than the gap sizes of the curved and Y-shaped waveguides. This large difference is attributed to a lowering of the scattering efficiency caused by wavefront tilting

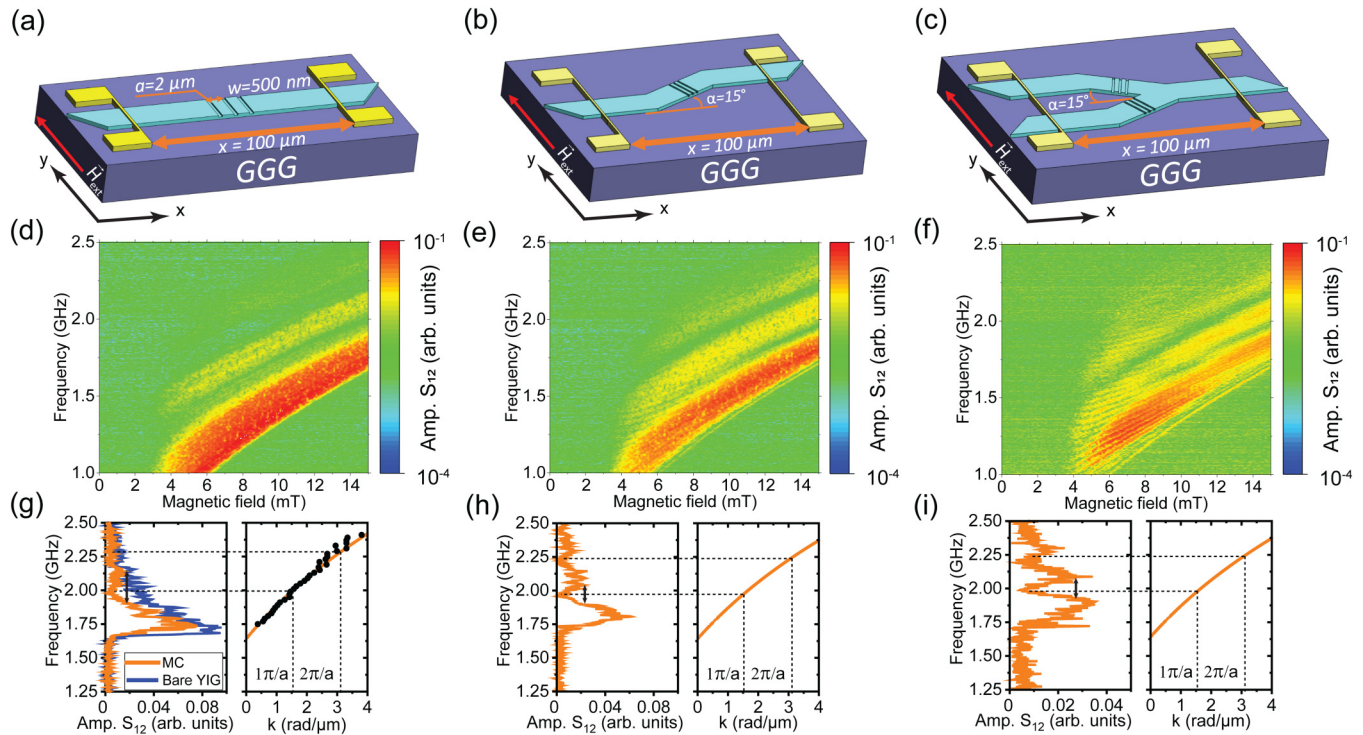


**FIG. 1.** (a)–(c) Schematic of the measurement geometry. The devices consist of microwave antennas and straight, curved, and Y-shaped YIG waveguides with magnonic crystals. The waveguide width is  $10\text{ }\mu\text{m}$ . The crystals consist of three 15-nm-deep and 500-nm-wide airgrooves with a lattice constant of  $2\text{ }\mu\text{m}$ . The angle of the curve is  $15^\circ$ . Spin waves are excited by a  $1\text{-}\mu\text{m}$ -wide microwave antenna and detected by a second antenna or imaged by SNS-MOKE microscopy. The external magnetic field is applied along the  $y$  axis. (d)–(f) Contour plots of the  $S_{12}$  scattering parameter amplitude as a function of magnetic field for the three waveguides. (g)–(i) Corresponding line profiles taken at 15 mT. The arrows indicate the size of the first transmission gap. The orange lines in the right panels show the calculated spin-wave dispersions. In (g), experimental data points extracted from SNS-MOKE microscopy are also shown (black solid symbols). The vertical and horizontal dashed lines indicate the center frequencies of the transmission gaps and the corresponding wave vectors. For comparison, a reference spectrum (blue line) measured on a bare YIG waveguide without magnonic crystal is shown in (g).

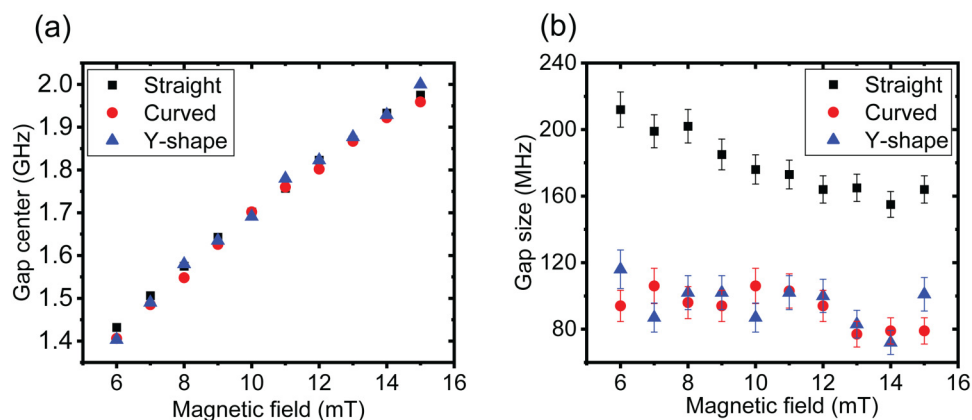


**FIG. 2.** (a) and (b) Center frequency and size of the first transmission gap as a function of external magnetic field for straight, curved, and Y-shaped YIG waveguides with magnonic crystals. The data are extracted from the spin-wave transmission spectra shown in Figs. 1(d)–1(f).



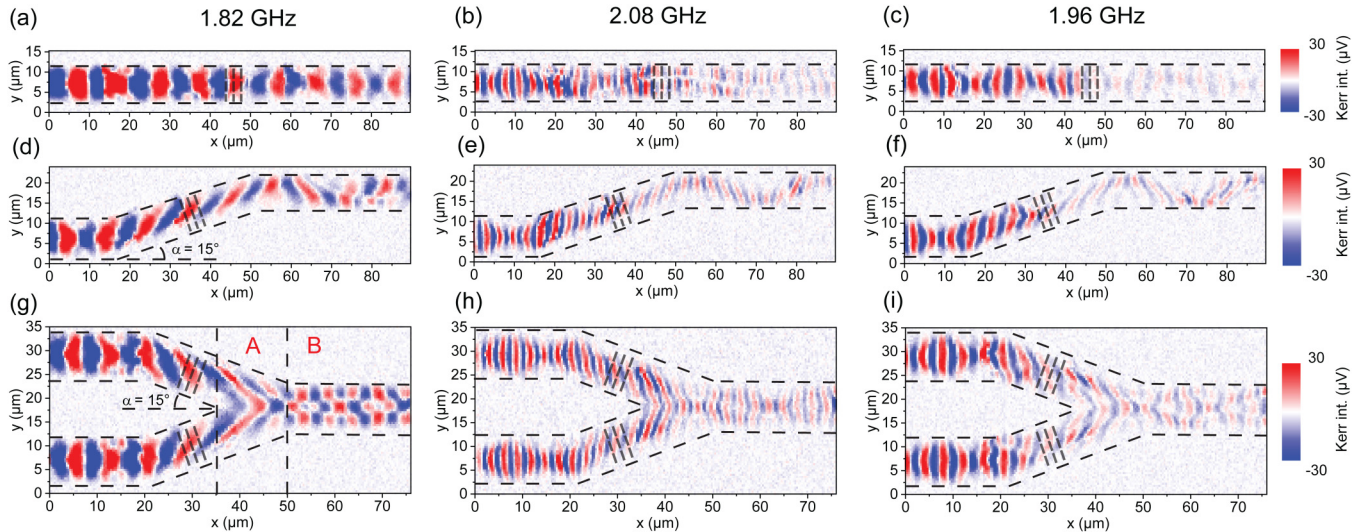


**FIG. 3.** SNS-MOKE microscopy images of propagating spin waves in (a)–(c) straight, (d)–(f) curved, and (g)–(i) Y-shaped YIG waveguides with magnonic crystals for  $f = 1.82$  and  $2.08$  GHz (outside the gap) and  $1.96$  GHz (inside the gap). The external magnetic field is  $16$  mT. The dashed lines indicate the edges of the waveguides.

with respect to the magnonic crystal in the waveguide curves (see Fig. 3) and the interference of different width modes in the straight and curved parts of the waveguides, which will be discussed later. With increasing bias field, the gap size of all crystals decreases. For instance, the gap size for the straight waveguide reduces from about  $200$  MHz at  $6$  mT to  $150$  MHz at  $15$  mT and  $120$  MHz at  $50$  mT (not shown). The evolution of the gap size with external magnetic field is caused by a flattening of the spin-wave dispersion relation.<sup>39</sup>

To visualize how spin waves propagate along the straight, curved, and Y-shaped waveguides, we conducted phase-resolved SNS-MOKE microscopy measurements at a frequency of  $1.82$  and  $2.08$  GHz (outside the gap) and  $1.96$  GHz (inside the gap) and a bias field of  $16$  mT. Figure 3 summarizes the results. Spin waves at  $f = 1.82$  GHz efficiently propagate along all waveguides with little signal decay. By fitting the spin-wave amplitude recorded on the straight waveguide to  $C \exp(-|x|/l_d) \sin(2\pi x/\lambda + \phi)$ , with  $\lambda$  the wavelength and  $\phi$  a phase offset, we extract a decay length  $l_d = 170 \mu\text{m}$ . This result indicates that the magnonic crystal hardly affects the transmission of spin waves outside the gap. The spin-wave signal at  $f = 2.08$  GHz remains strong also, but it decays faster compared to  $f = 1.82$  GHz because of a shortening of the spin-wave decay length with increasing frequency. At  $f = 1.96$  GHz, i.e., inside the transmission gap, the spin-wave signal is suppressed after the magnonic crystal, in agreement with the broadband spin-wave spectroscopy measurements in Fig. 1.

Now we discuss the interference and interconversion between different width modes. In the straight waveguide, a symmetric spin-wave profile with a diamond-like pattern is imaged. This profile is produced by the interference of  $n = 1$  and  $n = 3$  width modes, where  $n$  is the mode quantization number. Interference of the two width modes leads to a self-focusing effect, which is better visible

in Fig. 3 for  $f = 1.96$  and  $f = 2.08$  GHz. We calculated the dispersion of the  $k_{n,y} = n\pi/w$  width modes using Eq. (1) (Fig. 4). From these calculations, we estimated the length ( $L$ ) of the beating pattern arising from  $k_1$  and  $k_3$  wave interference using  $L = 2\pi/|k_3 - k_1|$ . This gives  $L = 22.4 \mu\text{m}$  and  $L = 27.3 \mu\text{m}$  for  $f = 1.96$  and  $f = 2.08$  GHz, respectively, in good agreement with

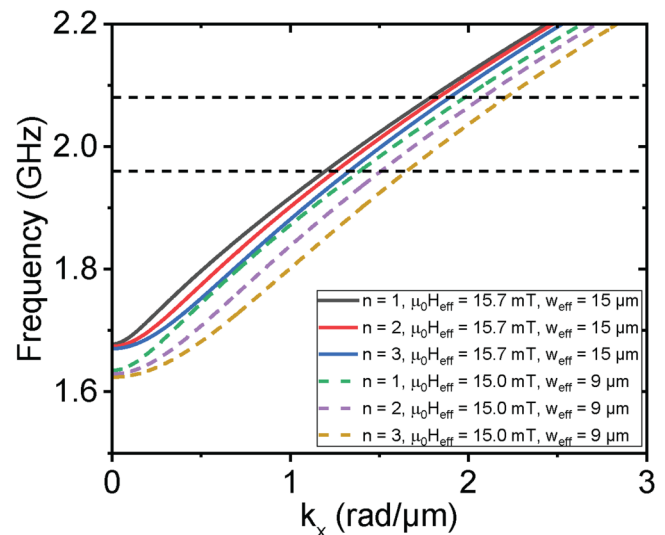


**FIG. 4.** Frequency of width modes with  $n = 1$ – $3$  as a function of wavevector  $k_x$  (along the waveguide). The lines represent the dispersions for regions A and B in the Y-shaped waveguide. The effective fields in A and B are taken from micromagnetic simulations.

the experiments. When spin waves propagate along a curve in the waveguide, the interference pattern changes from diamond-like to zigzag-like. The asymmetric zigzag-like intensity distribution is caused by the superposition of  $n = 1$  and  $n = 2$  width modes.<sup>40</sup> Generally, even width modes cannot be excited directly by a microwave antenna in straight waveguides because of the homogenous excitation field along the stripe. However, breaking of the translational symmetry in waveguide curves enables conversions between odd and even width modes.<sup>40</sup> In the Y-shaped structure,  $n = 1$  and  $n = 3$  width modes propagate along the straight arms and convert to  $n = 1$  and  $n = 2$  modes in the curves. When entering the joint region [marked by A in Fig. 3(g)], an increase of the effective magnetic field caused by the larger waveguide width in A shifts the dispersion curve up (see Fig. 4). At  $f = 1.82$  GHz, the  $n = 1$  width mode nearly vanishes in region A while the  $n = 2$  mode converts back to the  $n = 3$  mode after the two waveguides merge into one (region marked by B). For higher frequency, e.g.,  $f = 2.08$  GHz, both the  $n = 1$  and  $n = 2$  width modes exist in region A and they convert back to the  $n = 1$  and  $n = 3$  modes in region B.

#### IV. CONCLUSION

In summary, we investigated spin-wave transport in nanometer-thick YIG waveguides with integrated magnonic crystals using broadband spin-wave spectroscopy and SNS-MOKE microscopy. We observe deep and wide transmission gaps with sizes up to 200 MHz and low spin-wave transmission losses at allowed frequencies. The gaps are tunable by varying the external magnetic field or changing the waveguide shape. In straight, curved, and Y-shaped waveguides, we find symmetric and asymmetric mode profiles originating from the interference and interconversion between odd and even width modes. Low-loss and active control of spin-wave transmission in microscopic waveguides with integrated magnonic crystals offers perspectives for the design of spin-wave circuits.<sup>40–42</sup>

#### ACKNOWLEDGMENTS

This work was supported by the Academy of Finland (Grant Nos. 316857 and 325480). N. Kuznetsov acknowledges financial support from the Magnus Ehrnrooth Foundation. Lithography was performed at the OtaNano-Micronova Nanofabrication Centre, supported by Aalto University. Computational resources were provided by the Aalto Science-IT project.

#### AUTHOR DECLARATIONS

##### Conflict of Interest

The authors have no conflicts to disclose.

##### Author Contribution

H.J.Q. and S.v.D. led the project. N.K. fabricated the devices and perform broadband spin-wave spectroscopy measurements. N.K. and L.F. performed the SNS-MOKE measurements. N.K., H.J.Q., and S.v.D. wrote the manuscript. All authors discussed the results.

**Nikolai Kuznetsov:** Conceptualization (equal); Investigation (equal); Methodology (equal); Validation (equal); Visualization (equal); Writing – original draft (equal). **Huajun Qin:** Conceptualization (equal); Funding acquisition (equal); Investigation (equal); Methodology (equal); Supervision (equal); Writing – review & editing (equal). **Lukáš Flajšman:** Investigation (equal); Methodology (equal); Visualization (equal). **Sebastiaan van Dijken:** Conceptualization (equal); Funding acquisition (equal); Project administration (equal); Supervision (equal); Writing – review & editing (equal).

#### DATA AVAILABILITY

The data that support the findings of this study are available from the corresponding authors upon reasonable request.

#### REFERENCES

- <sup>1</sup>V. Kruglyak, S. Demokritov, and D. Grundler, “Magnonics,” *J. Phys. D: Appl. Phys.* **43**, 264001 (2010).
- <sup>2</sup>A. V. Chumak, V. I. Vasyuchka, A. A. Serga, and B. Hillebrands, “Magnon spintronics,” *Nat. Phys.* **11**, 453–461 (2015).
- <sup>3</sup>A. Chumak, A. Serga, and B. Hillebrands, “Magnonic crystals for data processing,” *J. Phys. D: Appl. Phys.* **50**, 244001 (2017).
- <sup>4</sup>A. Mahmoud, F. Ciubotaru, F. Vanderveken, A. V. Chumak, S. Hamdioui, C. Adelmann, and S. Cotozana, “Introduction to spin wave computing,” *J. Appl. Phys.* **128**, 161101 (2020).
- <sup>5</sup>A. Barman, G. Gubbiotti, S. Ladak, A. O. Adeyeye, M. Krawczyk, J. Gräfe, C. Adelmann, S. Cotozana, A. Naeemi, V. I. Vasyuchka, and B. Hillebrands, “The 2021 magnonics roadmap,” *J. Phys.: Condens. Matter* **33**, 413001 (2021).
- <sup>6</sup>P. Pirro, V. I. Vasyuchka, A. A. Serga, and B. Hillebrands, “Advances in coherent magnonics,” *Nat. Rev. Mater.* **6**, 1114–1135 (2021).
- <sup>7</sup>A. Chumak, P. Kabos, M. Wu, C. Abert, C. Adelmann, A. Adeyeye, J. Åkerman, F. Aliev, A. Anane, A. Awad, and C. H. Back, “Advances in magnetics roadmap on spin-wave computing,” *IEEE Trans. Magn.* **58**, 0800172 (2022).
- <sup>8</sup>A. Chumak, A. Serga, B. Hillebrands, and M. Kostylev, “Scattering of backward spin waves in a one-dimensional magnonic crystal,” *Appl. Phys. Lett.* **93**, 022508 (2008).
- <sup>9</sup>A. Chumak, A. Serga, S. Wolff, B. Hillebrands, and M. Kostylev, “Scattering of surface and volume spin waves in a magnonic crystal,” *Appl. Phys. Lett.* **94**, 172511 (2009).
- <sup>10</sup>C. L. Ordóñez-Romero, Z. Lazcano-Ortiz, A. Drozdovskii, B. Kalinikos, M. Aguilar-Huerta, J. Domínguez-Juárez, G. Lopez-Maldonado, N. Qureshi, O. Kolokoltsev, and G. Monsivais, “Mapping of spin wave propagation in a one-dimensional magnonic crystal,” *J. Appl. Phys.* **120**, 043901 (2016).
- <sup>11</sup>A. A. Nikitin, A. B. Ustinov, A. A. Semenov, A. V. Chumak, A. A. Serga, V. I. Vasyuchka, E. Lähderanta, B. A. Kalinikos, and B. Hillebrands, “A spin-wave logic gate based on a width-modulated dynamic magnonic crystal,” *Appl. Phys. Lett.* **106**, 102405 (2015).
- <sup>12</sup>P. Frey, A. A. Nikitin, D. A. Bozhko, S. A. Bunyaev, G. N. Kakazei, A. B. Ustinov, B. A. Kalinikos, F. Ciubotaru, A. V. Chumak, Q. Wang, and V. S. Tiberkevich, “Reflection-less width-modulated magnonic crystal,” *Commun. Phys.* **3**, 17 (2020).
- <sup>13</sup>H. Merbouche, M. Collet, M. Evelt, V. E. Demidov, J. L. Prieto, M. Munoz, J. Ben Youssef, G. de Loubens, O. Klein, S. Xavier, and O. D’Allivy Kelly, “Frequency filtering with a magnonic crystal based on nanometer-thick yttrium iron garnet films,” *ACS Appl. Nano Mater.* **4**, 121–128 (2021).
- <sup>14</sup>M. Inoue, A. Baryshev, H. Takagi, P. B. Lim, K. Hatafuku, J. Noda, and K. Togo, “Investigating the use of magnonic crystals as extremely sensitive magnetic field sensors at room temperature,” *Appl. Phys. Lett.* **98**, 132511 (2011).
- <sup>15</sup>V. Bessonov, M. Mruczkiewicz, R. Gieniusz, U. Guzowska, A. Maziewski, A. Stognij, and M. Krawczyk, “Magnonic band gaps in YIG-based

one-dimensional magnonic crystals: An array of grooves versus an array of metallic stripes," *Phys. Rev. B* **91**, 104421 (2015).

<sup>16</sup>T. Goto, K. Shimada, Y. Nakamura, H. Uchida, and M. Inoue, "One-dimensional magnonic crystal with Cu stripes for forward volume spin waves," *Phys. Rev. Appl.* **11**, 014033 (2019).

<sup>17</sup>A. Chumak, T. Neumann, A. Serga, B. Hillebrands, and M. Kostylev, "A current-controlled, dynamic magnonic crystal," *J. Phys. D: Appl. Phys.* **42**, 205005 (2009).

<sup>18</sup>A. V. Chumak, V. S. Tiberkevich, A. D. Karenowska, A. A. Serga, J. F. Gregg, A. N. Slavin, and B. Hillebrands, "All-linear time reversal by a dynamic artificial crystal," *Nat. Commun.* **1**, 141 (2010).

<sup>19</sup>A. Sadovnikov, A. Grachev, S. Sheshukova, Y. P. Sharaevskii, A. Serdobintsev, D. Mitin, and S. Nikitov, "Magnon straintronics: Reconfigurable spin-wave routing in strain-controlled bilateral magnetic stripes," *Phys. Rev. Lett.* **120**, 257203 (2018).

<sup>20</sup>A. B. Ustinov and B. A. Kalinikos, "Multiferroic periodic structures based on magnonic crystals for electronically tunable microwave devices," *Tech. Phys. Lett.* **40**, 568–570 (2014).

<sup>21</sup>M. A. Morozova, S. V. Grishin, A. V. Sadovnikov, D. V. Romanenko, Y. P. Sharaevskii, and S. A. Nikitov, "Tunable bandgaps in layered structure magnonic crystal-ferroelectric," *IEEE Trans. Magn.* **51**, 2802504 (2015).

<sup>22</sup>A. B. Ustinov, A. V. Drozdovskii, A. A. Nikitin, A. A. Semenov, D. A. Bozhko, A. A. Serga, B. Hillebrands, E. Lähderanta, and B. A. Kalinikos, "Dynamic electromagnonic crystal based on artificial multiferroic heterostructure," *Commun. Phys.* **2**, 137 (2019).

<sup>23</sup>B. Rana and Y. Otani, "Towards magnonic devices based on voltage-controlled magnetic anisotropy," *Commun. Phys.* **2**, 90 (2019).

<sup>24</sup>H. Qin, R. Dreyer, G. Woltersdorf, T. Taniyama, and S. van Dijken, "Electric-field control of propagating spin waves by ferroelectric domain-wall motion in a multiferroic heterostructure," *Adv. Mater.* **33**, 2100646 (2021).

<sup>25</sup>H. Qin, G.-J. Both, S. J. Hämäläinen, L. Yao, and S. van Dijken, "Low-loss YIG-based magnonic crystals with large tunable bandgaps," *Nat. Commun.* **9**, 5445 (2018).

<sup>26</sup>H. Qin and S. van Dijken, "Nanometer-thick YIG-based magnonic crystals: Bandgap dependence on groove depth, lattice constant, and film thickness," *Appl. Phys. Lett.* **116**, 202403 (2020).

<sup>27</sup>V. E. Demidov, S. O. Demokritov, K. Rott, P. Krzysteczko, and G. Reiss, "Self-focusing of spin waves in permalloy microstrips," *Appl. Phys. Lett.* **91**, 252504 (2007).

<sup>28</sup>M. Collet, O. Gladii, M. Evelt, V. Bessonov, L. Soumah, P. Bortolotti, S. O. Demokritov, Y. Henry, V. Cros, M. Bailleul, V. E. Demidov, and A. Anane, "Spin-wave propagation in ultra-thin YIG based waveguides," *Appl. Phys. Lett.* **110**, 092408 (2017).

<sup>29</sup>Q. Wang, B. Heinz, R. Verba, M. Kewenig, P. Pirro, M. Schneider, T. Meyer, B. Lägel, C. Dubs, T. Brächer, and A. V. Chumak, "Spin pinning and spin-wave

dispersion in nanoscopic ferromagnetic waveguides," *Phys. Rev. Lett.* **122**, 247202 (2019).

<sup>30</sup>B. Heinz, T. Brächer, M. Schneider, Q. Wang, B. Lägel, A. M. Friedel, D. Breitbach, S. Steinert, T. Meyer, M. Kewenig, C. Dubs, P. Pirro, and A. V. Chumak, "Propagation of spin-wave packets in individual nanosized yttrium iron garnet magnonic conduits," *Nano Lett.* **20**, 4220–4227 (2020).

<sup>31</sup>Q. Wang, M. Kewenig, M. Schneider, R. Verba, F. Kohl, B. Heinz, M. Geilen, M. Mohseni, B. Lägel, F. Ciubotaru, C. Adelman, C. Dubs, S. D. Cotoana, O. V. Dobrovolskiy, T. Brächer, P. Pirro, and A. V. Chumak, "A magnonic directional coupler for integrated magnonic half-adders," *Nat. Electron.* **3**, 765–774 (2020).

<sup>32</sup>B. Heinz, Q. Wang, M. Schneider, E. Weiß, A. Lentfert, B. Lägel, T. Brächer, C. Dubs, O. V. Dobrovolskiy, P. Pirro, and A. V. Chumak, "Long-range spin-wave propagation in transversely magnetized nano-scaled conduits," *Appl. Phys. Lett.* **118**, 132406 (2021).

<sup>33</sup>Y. V. Khivintsev, V. K. Sakharov, A. V. Kozhevnikov, G. M. Dudko, Y. A. Filimonov, and A. Khitun, "Spin waves in YIG based magnonic networks: Design and technological aspects," *J. Magn. Magn. Mater.* **545**, 168754 (2022).

<sup>34</sup>H. Qin, R. B. Holländer, L. Flajšman, F. Hermann, R. Dreyer, G. Woltersdorf, and S. van Dijken, "Nanoscale magnonic Fabry-Pérot resonator for low-loss spin-wave manipulation," *Nat. Commun.* **12**, 2293 (2021).

<sup>35</sup>R. Damon and J. Eshbach, "Magnetostatic modes of a ferromagnet slab," *J. Phys. Chem. Solids* **19**, 308–320 (1961).

<sup>36</sup>B. Kalinikos and A. Slavin, "Theory of dipole-exchange spin wave spectrum for ferromagnetic films with mixed exchange boundary conditions," *J. Phys. C* **19**, 7013 (1986).

<sup>37</sup>Z. Zhang, M. Vogel, J. Holanda, J. Ding, M. B. Jungfleisch, Y. Li, J. E. Pearson, R. Divan, W. Zhang, A. Hoffmann, Y. Nie, and V. Novosad, "Controlled inter-conversion of quantized spin wave modes via local magnetic fields," *Phys. Rev. B* **100**, 014429 (2019).

<sup>38</sup>A. Vansteenkiste, J. Leliaert, M. Dvornik, M. Helsen, F. Garcia-Sanchez, and B. Van Waeyenberge, "The design and verification of MuMax3," *AIP Adv.* **4**, 107133 (2014).

<sup>39</sup>H. Qin, S. J. Hämäläinen, K. Arjas, J. Witteveen, and S. van Dijken, "Propagating spin waves in nanometer-thick yttrium iron garnet films: Dependence on wave vector, magnetic field strength, and angle," *Phys. Rev. B* **98**, 224422 (2018).

<sup>40</sup>P. Clausen, K. Vogt, H. Schultheiss, S. Schäfer, B. Obry, G. Wolf, P. Pirro, B. Leven, and B. Hillebrands, "Mode conversion by symmetry breaking of propagating spin waves," *Appl. Phys. Lett.* **99**, 162505 (2011).

<sup>41</sup>K. Vogt, H. Schultheiss, S. Jain, J. Pearson, A. Hoffmann, S. Bader, and B. Hillebrands, "Spin waves turning a corner," *Appl. Phys. Lett.* **101**, 042410 (2012).

<sup>42</sup>A. Sadovnikov, C. Davies, V. Kruglyak, D. Romanenko, S. Grishin, E. Beginin, Y. P. Sharaevskii, and S. Nikitov, "Spin wave propagation in a uniformly biased curved magnonic waveguide," *Phys. Rev. B* **96**, 060401 (2017).